HHS Public Access

Author manuscript

Neuroscience. Author manuscript; available in PMC 2024 August 01.

Published in final edited form as:

Neuroscience. 2023 August 01; 524: 181–196. doi:10.1016/j.neuroscience.2023.06.002.

Nucleus accumbens shell neurons encode the kinematics of reward approach locomotion

David Levcik[1,4,#], **Adam H. Sugi**[1,2,3,#], **Marcelo Aguilar-Rivera**[5,#], **José A. Pochapski**[1,2], **Gabriel Baltazar**[1,2,3], **Laura N. Pulido**[1,2], **Cyrus Villas Boas**[1], **Romulo Fuentes-Flores**[6], **Saleem M. Nicola**[7,8], **Claudio Da Cunha**[1,2,3,*]

[1.]Laboratório de Fisiologia e Farmacologia do Sistema Nervoso Central, Universidade Federal do Paraná, 81531-980, Curitiba, Brazil

[2.]Department of Pharmacology, Universidade Federal do Paraná, Curitiba, Brazil

[3.]Department of Biochemistry, Universidade Federal do Paraná, Curitiba Brazil

[4.]Institute of Physiology of the Czech Academy of Sciences, Videnska 1083, 142 20, Prague, Czech Republic

[5.]Department of Bioengineering, University of California, 9500 Gilman Drive MC 0412, La Jolla, San Diego, 92093, USA

[6.]Departamento de Neurociencia, Facultad de Medicina, Universidad de Chile, Av. Independencia 1027, Independencia 8380453, Santiago, Chile

[7.]Department of Neuroscience, Albert Einstein College of Medicine, 1300 Morris Park Ave, Bronx, New York, 10461 USA

[8.]Department of Psychiatry, Albert Einstein College of Medicine, New York, USA

Abstract

The nucleus accumbens (NAc) is considered an interface between motivation and action, with NAc neurons playing an important role in promoting reward approach. However, the encoding by NAc neurons that contributes to this role remains unknown. We recorded 62 NAc neurons in male Wistar rats (n = 5) running towards rewarded locations in an 8-arm radial maze. Variables related to locomotor approach kinematics were the best predictors of the firing rate for most NAc neurons. Nearly 18% of the recorded neurons were inhibited during the entire approach run (locomotion-off cells), suggesting that reduction in firing of these neurons promotes initiation of locomotor approach. 27% of the neurons presented a peak of activity during acceleration followed

*Corresponding author dacunha.claudio@gmail.com.

#The authors presented equally important contributions.

Author contributions statement

D.L., M.A.-R., R.F.-F. and C.D.C. designed research; D.L., A.H.S., J.A.P., G.B., L.N.P., and C.V.B. performed experiments; D.L., A.H.S., M.A.-R., J.A.P., G.B., L.N.P., C.V.B., S.M.N. and C.D.C. analyzed data; D.L., A.H.S., R.F.-F., S.M.N. and C.D.C. wrote the manuscript. All authors reviewed the manuscript.

by a valley during deceleration (acceleration-on cells). Together, these neurons accounted for most of the speed and acceleration encoding identified in our analysis. In contrast, a further 16% of neurons presented a valley during acceleration followed by a peak just prior to or after reaching reward (deceleration-on cells). These findings suggest that these three classes of NAc neurons influence the time course of speed changes during locomotor approach to reward.

Keywords

Nucleus accumbens; reward approach; kinematics encoding; locomotor speed; initiation of action

Introduction

A major function of NAc neurons is to promote the vigorous pursuit of rewards (Nicola, 2007; Salamone and Correa, 2012; Nicola, 2016). Inhibition of dopamine neurotransmission in the NAc impairs performance of high-effort tasks while leaving lower-effort tasks relatively unaffected (Salamone et al., 1999), biases animals to choose the less effortful option (Salamone et al., 1994; Cousins et al., 1996; Hauber and Sommer, 2009), and reduces the probability of engaging in locomotor approach responses to reward-predictive cues (Nicola, 2010; Ambroggi et al., 2011). Consistent with these observations, many NAc neurons are briefly excited by reward-predictive cues (Nicola et al., 2004; Atallah et al., 2014; Gmaz et al., 2018), and these excitations predict the vigor of the approach response – specifically, the neuron activity is higher when the latency to initiate approach will be shorter and the speed of approach greater (McGinty et al., 2013; Morrison et al., 2017). This form of encoding likely contributes causally to vigorous performance of cued approach tasks (du Hoffmann and Nicola, 2014; Caref and Nicola, 2018).

Although NAc cue-evoked firing responses that begin prior to movement onset compellingly link reward prediction to effort exertion, it remains unclear whether NAc neuronal activity that continues throughout the movement represents parameters related to movement such as speed or direction. This question is not readily answered with animals in standard-sized operant chambers because the short movement distance limits the maximal speed and the time taken to complete the movement, both of which limit the dynamic range across which speed varies.

In contrast, in maze or runway tasks in which subjects must move long distances (e.g. 1 m or greater) to rewarded locations, it takes several seconds to complete the approach and the maximal speed is higher, allowing sufficient dynamic range to relate neural activity to movement throughout the run. Although NAc neuronal activity has been measured in such tasks (Lavoie and Mizumori, 1994; Shibata et al., 2001; Mulder et al., 2004; Mulder et al., 2005; German and Fields, 2007; Khamassi et al., 2008; van der Meer and Redish, 2009; van der Meer et al., 2010; Atallah, et al., 2014; Gmaz, et al., 2018), the relationship between neuronal activity and the kinematic parameters of locomotion has not been systematically investigated, despite anecdotal reports that NAc neurons' firing reflects locomotor speed (Sjulson et al., 2018).

To address this deficiency, we recorded from NAc shell neurons as rats performed an 8-arm radial maze task in which 3 arms were consistently rewarded, and animals had to traverse long distances to obtain rewards. We focused on the NAc shell because it receives a prominent projection from the hippocampus (Groenewegen et al., 1987; Brog et al., 1993; Floresco et al., 2001), which may carry information related to navigation and movement direction (Albertin et al., 2000). It is unknown whether NAc shell neurons integrate this information with kinematic parameters such as speed and acceleration. We found that although some neurons did represent movement direction, speed and proximity to the rewarded target were more strongly and consistently encoded by many NAc shell neurons during reward approach, and that neuronal activity predicted speed approximately 100 ms in advance. In addition, we found 3 classes of neurons with distinctive patterns of activity, including peaks of firing that occurred throughout the time course of locomotion, that together could account for the control of the start of the approach run and the timing of acceleration and deceleration.

Experimental Procedures

Subjects.

We used adult male Wistar rats that were three months old at the beginning of the experiment. The rats were housed in groups of 4 per cage during behavioral training. The 5 rats that fulfilled the performance criteria were housed individually after surgery to minimize the risk of damaging the implanted electrophysiological microdrives. The rats were maintained in a temperature-controlled room (22 ± 2 °C) with a 12-hr light/dark cycle (lights on at 7:00 am). Access to water was allowed for one hour per day, and access to food was restricted to maintain the rats' body weight at 90% of their free-feeding weight (290 - 340 g). All experimental procedures were in agreement with the Brazilian and International legislation for animal care (Law N° 11.794 of October 8, 2008; EC Council Directive of November 24, 1986; 86/609/EEC). The project was approved by the Animal Care and Use Committee of the Federal University of Parana State. The experiments were conducted in accordance with ARRIVE guidelines.

Apparatus.

We used for behavioral training a stainless steel eight-arm radial maze, which had a surface covered with black contact paper. Each arm (62 cm x 13 cm) and the central platform (an octagon with a 30 cm diameter) were elevated 60 cm above the floor. The walls of all arms were 5 cm high. One or four drops (25 μl per drop) of chocolate milk were delivered at the ends of reward arms before the start of each trial. A white curtain was installed around the maze and several salient visual cues (black felt geometrical shapes) were attached to it and remained in the same locations throughout behavioral training and experiments. Four light bulbs (15 W) were spaced equally on a metal frame (70 x 70 cm) above the center of the maze. This metal frame also served as a support for a motorized commutator (Plexon, USA), a camera (Allied Vision Technologies GmbH, Germany) connected to the main computer, and an amplifier (Plexon, USA).

Behavioral procedures.

All rats were handled (5 min/day) by the experimenter for three consecutive days before the start of behavioral pre-training. During pre-training, rats were habituated to the maze and the chocolate milk reward by placing them at the end of one arm and letting them drink the chocolate milk from the reward receptacle.

After the pre-training phase, rats were trained to collect drops of chocolate milk consistently located at the ends of the same three arms of an eight-arm radial arm maze (Fig. 1A). The positions of these three reward arms were counterbalanced among rats and were chosen in a pseudorandom manner so that two adjacent arms were never baited. In the same-reward group (n = 2), all reward arms (X, Y and Z) contained 4 drops of chocolate milk (100 μl) in 100% of trials. In the different-reward group (n = 3), one of the reward arms contained four drops (100 μl) of chocolate milk in 100% of trials (high reward), another reward arm contained four drops (100 μl) in 66.7% of trials (medium reward), and the last reward arm contained one drop (25 μl) in 100% of trials (low reward). The rewarded locations, and the reward amounts and probabilities, remained constant for a given rat throughout training and experiments.

A fourth arm was consistently used as a resting platform, where the rats were placed and restricted between trials. The other four arms were used as starting positions (S1 - S4, Fig. 1A). The rats underwent nine trials per day. Two starting positions were alternated in a pseudorandom order, one used three times and the other two times. Each trial finished when all rewards were collected or after 5 min elapsed. The rats were trained five days per week until they reached the following criteria in three consecutive training days: a) no more than 20% reference memory errors (entering a non-reward arm); b) the high reward arm (4 drops, 100% probability) is the last choice in no more than 20% of trials; and c) the low reward arm (1 drop, 100% probability) is the first choice in no more than 20% of trials. Criteria b and c were applied only to the different-reward group. The rats took 40 to 50 training days to achieve these criteria. For the purposes of our analyses, we merged data from both the same reward and different reward groups as we observed that reward approach behavior was highly stereotyped across all rats after the long training period. In particular, *speed* vs time trajectories were similar for the two groups and did not substantially differ across different start/end arm combinations. We did not further analyze the impact of expected or past reward on firing as we did not have enough samples (visits of individual arms of different value) for a robust analysis.

After training, rats underwent surgery to implant recording electrodes arranged in a microdrive above the NAc shell. After recovery, they were re-trained to the pre-surgery level of performance, which took approximately seven days. During these re-training sessions and the following recording sessions, 12 trials per session were carried out. After completion of recordings from NAc neurons, rats' brains were removed for histological staining. See details related to surgical, recording, and histological procedures in Supplemental Experimental Procedures.

Neuronal activity analysis.

A recording session consisted of 12 trials. In each trial, the rats should visit the three reward arms. The rats usually approached the reward areas of the three reward arms only once. Each approach was defined as a run – when the rat ran from the distal end of one arm towards the reward area of a reward arm (Fig. 1A). Trained rats performed few visits to non-reward arms, and only data from approaches to reward arms were analyzed. For most analyses, the time window analyzed for each run extended from 1 s before locomotion onset to 1 s after the locomotion end. Taking advantage of the fact that the animals' behavior across runs was generally consistent, locomotion onset was defined as the first time point in which the *speed* of the animal reached 20 cm/s before the peak speed of the run (Fig. 1B). Locomotion end was set as the first point at which the *speed* dropped below 10 cm/s. We restricted our analysis to stereotyped trajectories to the reward defined by an efficiency criterion, which was calculated as the ratio of the distance traveled in the run to the length of the ideal path (from the end of one arm to the reward area of another arm). Incomplete runs, i.e. the rat enters the arm but does not reach the end of it, result in ratios <1. To eliminate most such runs, and runs in which the animal deviated substantially from a direct trajectory to the end of the reward arm, runs with high efficiency (ratio < 0.8) or low efficiency (ratio > 1.2) were discarded. Of a total of 2587 runs, 877 were eliminated because they were visits to never-rewarded arms, re-visits to arms where reward had already been collected, or the run did not meet the efficiency criteria.

Generalized linear model (GLM).

The goal of the multiple regression analysis was to evaluate which performance-related parameters can be used to predict neuronal firing rate. A GLM was calculated with the firing rate (spikes/100-ms bin) as the dependent variable and 14 parameters as predictors (independent variables; Supplemental Tab. S1). Pearson correlations (r) among pairs of predictor variables were calculated and, for the pairs that showed r > 0.8, one of them was excluded (Supplemental Fig. S1).

Different continuous variables were extracted from the coordinates tracked in the recorded videos. The rat's locations were tracked at 30 frames per second. However, to match the neuronal data that were binned at 100 ms, an interval of 3 frames was used (3 frames = 100 ms interval). Firing rate, *speed* and *acceleration* were smoothed by a sliding average window of 300 ms (Kropff et al., 2015; Rueda-Orozco and Robbe, 2015). The β values were calculated with the MATLAB *glmfit* function. The multiple regression assumed a normal distribution for the data and the identity link function was used to estimate the β value for each parameter.

The GLM followed the equation:

$$Y(t) = \beta 0 + \beta 1 x1(t) + \beta 2 x2(t) + \ldots + \beta n x n(t) + \varepsilon \quad (1)$$

where $Y(t)$ is the predicted firing rate at time t, βn is the weight of the predictor n, $xn(t)$ is the value of the predictor n at time t, and ε is the error term. For each neuron, the model was trained and tested by the fivefold cross validation method (Engelhard et al., 2019) as follows. The data from all the runs (*speed, acceleration*, firing rate, etc.) were divided into

5 parts with the same number of runs. The runs used in each part were randomly selected. The model was trained and tested five times with 4/5 of the total data, and the ability of the model to predict the remaining 1/5 of the data was assessed by correlating the predicted data to the actual data. Always, a different combination of the data was used as training and test data (Supplemental Fig. S2).

The mean of the r^2 values obtained from the five correlations (r^2_{mean}) was considered the mean fraction of variance explained by the full model (FM, the model with all predictors included). The significance of the model was evaluated by comparing the r^2_{mean} to the distribution of r^2_{mean} values generated by models trained with shuffled neuronal data (100 shuffled models per neuron, n = 62 neurons). Neurons for which the model explained the actual data better than the 99th percentile of the shuffled models were classified as having their firing rates significantly explained by the encoding model.

Contribution of each predictor to the GLM.

To evaluate which variables had a significant contribution to the full model (FM), only neurons significantly explained by the FM were analyzed. To calculate the contribution of each of the variables (var) to the FM, the FM was compared to the full model less the selected variable (FM – var). The mean fraction of the variance explained by FM - var was calculated as the mean r^2 of the correlation between the output of the FM - var and the real firing data. These values were compared to the mean r^2 of the correlation between the FM and real firing data using Bonferroni-corrected t-tests. The contribution of a variable to the variance in firing rate was considered significant if $P < 0.01$.

Cross-correlogram analysis.

The aim of this analysis was to test whether changes in firing rate preceded or followed changes in the animal's speed. First, based on each neuron's Pearson's correlation between speed and firing rate, we divided neurons into two groups, those with positive correlations between firing rate and speed, and those with negative correlations. Only neurons with correlations higher or lower than the 99.5th percentile of a bootstrapping distribution of Pearson's correlations were included in these groups (1000 correlations of shuffled spike times and speed were generated for each neuron). For each of the included neurons, the average speed before and after each spike (bins of 33 ms) was calculated to generate a normalized (z-scored) cross-correlogram. Finally, the time of the peak of each cross-correlogram was identified and then compared to zero (one-sample t-test).

The two Gaussians model (2G).

The 2G model used fraction of time to complete a run as the only independent variable. Time during the run was normalized by dividing the periods from locomotion onset to the peak of speed and from the peak of speed to locomotion end into 10 bins each. On average, the bin width was ~150 ms. The time windows starting 1.05 s before locomotion onset to locomotion onset, and from locomotion end to the 1.05 s after locomotion end, were each divided in 7 bins (150 ms each). The firing rate during each bin was calculated and z-transformed.

The 2G model followed the equation:

$$Y_{(t)} = G1_{(t)} + G2_{(t)} + \mathrm{BL}$$

where $Y(t)$ is the predicted firing rate at time t, $G1$ is the Gaussian equation for the peak of the curve, $G2$ is the equation for the valley of the curve, and BL is the baseline activity.

The Gaussian equations ($G_{(t)}$) used were:

$$G1_{(t)} = H1e^{-n(\frac{X_{(t)} - F1}{W1})^2}, \; G2_{(t)} = -H2e^{-n(\frac{X_{(t)} - F2}{W2})^2}$$

where H, F, and W are constants with the following meaning: H represents the amplitude of the Gaussian curve, which reflects the height ($H1$) and depth ($H2$) of the activity peak and the valley, respectively. F is the bin where the Gaussian is centered. Therefore, $F1$ is the bin in which the neuron is most active, and $F2$ is the bin in which the neuron is least active. W is the standard deviation of each Gaussian, which reflects the durations of the activation peak ($W1$) and valley ($W2$). For each neuron, data from all runs were randomly split in two pools. One data pool was used to adjust these constants and the other pool was used to test the prediction power of the model. 2G constants were adjusted by using the Generalized Reduced Gradient (GRG) engine solver of Microsoft Excel to minimize the sum of the square roots of the difference between the firing rate recorded in each fraction of time and the firing rate predicted by the 2G model (Supplemental Fig. S6). Next, the r and P for the correlation between the firing rate predicted by the 2G model and the firing rate activity calculated with the other data pool was calculated. The 2G model was considered to significantly predict activity of a neuron when $P < 0.01$.

We analyzed the data and prepared figures using MATLAB R2021b (The Math Works, Inc.), GraphPad Prism 9 (GraphPad Software, Inc.), and CorelDRAW 2017 (CorelDRAW Graphics Suite).

Results

Behavioral task performance

Five rats were trained to collect chocolate milk rewards located in three arms of the 8-arm radial maze task (Fig. 1A). The same three arms were rewarded across sessions and experiments, and after extensive training (40 - 50 days), the rats rarely visited the non-reward arms. Furthermore, after consuming the reward in one arm, rats only occasionally revisited the arm in the same trial (Supplemental Table S3). Therefore, for each trial only the three approach runs towards the end of the reward arms were considered, while the runs to non-reward arms were not analyzed. Because traveled distances from the starting location to the reward location were long and constant, speed varied from locomotion start to locomotion end in a stereotyped way (Fig. 1B). Each run consisted of a single acceleration to peak speed followed by a deceleration to locomotion end at the reward location (i.e., along the way, rats did not stop). This consistent pattern of speed variation during each run allowed us to evaluate the relationship between kinematic variables and neuronal activity.

Unlike most tasks used to study approach behavior, no start cue was provided and each run was therefore self-initiated.

Speed and fraction of the run are the best predictors of NAc firing rate during approach behavior

Sixty-two NAc neurons were recorded while trained rats performed the radial arm maze task (Supplemental Tab. S1). To examine how NAc neurons encode kinematic parameters of locomotion, we considered the set of variables shown in Supplemental Table S2. We tested whether the firing rate of each neuron could be predicted with a generalized linear model (GLM) that used all these parameters as predictive variables. Prior to running the GLMs, we examined the correlation between pairs of variables and found that *fraction of the run, time* since locomotion onset, and *distance traveled* were strongly correlated with each other ($r > 0.8$, Supplemental Fig. S1). We therefore excluded *time* and *distance traveled* from the GLM analysis. In addition, *fraction of the run* and *acceleration* were correlated, but less strongly ($r = 0.6$). To assess whether one of these variables explained more of the variance in firing rate than the other, we conducted three separate GLM analyses for each neuron, one including both variables and the other two including either *fraction of the ran* or *acceleration*. We refer to these three GLMs as full models (FMs).

We first assessed the validity of the GLM that included both *fraction of the run* and *acceleration* using a five-fold validation method (Engelhard, et al., 2019). For each neuron, we computed the r^2_{mean}: the mean of the five r^2 values from the correlations between the modeled firing rates (obtained from running the GLM on $^4/_5$ of the data) and the remaining $^1/_5$ of the actual firing rate data (Supplemental Fig. S2). Representative examples comparing actual firing rate with the firing rate predicted by the FM are shown in Figure 2B. FMs predicted the changes in the firing rate of 39 units (63% of the neurons) with a r^2_{mean} greater than the correlation predicted by 99% of models that used shuffled data (Fig. 2A). The average r^2 across the 39 neurons ($r^2_{mean} \pm SEM$) was 0.156 ± 0.018. In the model in which the variable *acceleration* was excluded, 39 cells (63%) passed this criterion (Supplemental Fig. S3) and in the model in which the variable *fraction of the run* was excluded 36 cells (58%) passed this criterion (Supplemental Fig. S4). The similarity of the results across the three models indicates that neither *acceleration* nor *fraction of the run* explained a greater degree of the firing rate variance than the other. Roughly the same neurons were well fit by the three different models (34 neurons by all three models, 1 neuron only by the model without acceleration, 2 neurons only by the model without fraction of the run, and 2 neurons only by the model with both variables). In summary, in the majority of neurons, our GLMs predicted firing rate much better than chance and accounted for variance within the range reported by others (Gmaz, et al., 2018; Engelhard, et al., 2019).

To determine which independent variables accounted for a significant fraction of the variance in firing rate, for each neuron we ran the GLM with one variable excluded, and repeated this with each variable. Individually removing only two of the variables, *speed* and *fraction of the run*, significantly decreased the r^2_{mean} across neurons ($P < 0.01$, t-test, Fig. 2C,D). Removing *acceleration* had an effect that did not reach significance after correction for multiple comparisons (Fig. 2D); however, when the variable *fraction*

of the run (which was correlated with *acceleration*, r = 0.6) was excluded from the model, removing *acceleration* caused a significant decrease in r^2_{mean} (Supplemental Fig. S4). Furthermore, when *acceleration* was excluded from the model, removing the variable *fraction of the run* caused an even larger decrease in r^2_{mean} (Supplemental Fig. S3). This suggests that part of the predictive information carried by the variable *fraction of the run* that is encoded by the NAc neurons is the change in *acceleration* during the run.

To confirm that *speed* and *fraction of the run* strongly influence firing, we ran GLMs that included only these two independent variables. These models predicted the firing rate of 38 (61%) of the neurons with a r^2_{mean} greater than the coefficient generated in 99% of models using shuffled data. Thus, our GLM analysis reveals that the kinematic variables *speed acceleration* and *fraction of the run* are most strongly predictive of NAc firing activity. Finally, to further confirm our conclusion, we utilized an alternative analysis approach to determine which variables most robustly predict firing rate. We performed Least Absolute Shrinkage and Selection Operator (LASSO) regression using the entire set of variables shown in Supplemental Table S2 and Supplemental Figure S1 including multicollinear variables . LASSO eliminates those variables with the least predictive value from the model, revealing those variables that are most predictive of firing rate and selecting, in an unbiased way, from among multicollinear variables. The analysis confirmed that speed and fraction of the run are significant predictors for many (50% and 34%, respectively) of the recorded cells (Supplemental Figure S5). To gain insight into the degree to which parameters related to kinematics (speed, acceleration, and the time course of these variables) and movement direction are represented in the neurons activity, we categorized neurons as Kinematics neurons if one or more kinematics variables (speed, fraction of the run, acceleration, max speed, run duration, center distance, distance traveled, time) remained in the neuron's LASSO model, and Direction neurons if one or more direction variables (arm Z, arm Y, right, left, angle - center, head direction, head movement) remained. We found that 15 of 62 neurons were classified as Kinematics, 1 was classified as Direction, 33 were classified as both, and 13 were classified as neither. These results suggest that kinematics is represented in a large majority of neurons (48 of 62, 77%), and that many of these also represented some aspect of movement direction. Interestingly, speed remained in the most LASSO models, and its correlated variable distance from center also remained in many neurons. These results suggest that speed is commonly represented by NAc neurons, consistent with the GLM results. In addition, fraction of the run remained in far more LASSO models than the correlated variable acceleration, suggesting that fraction of the run better predicted firing rate than acceleration. Together, speed, fraction of the run and center distance were responsible for the bulk of the Kinematics representation, whereas Direction representation was more dispersed among the various Direction variables. Finally, trial remained in many models, suggesting that some neurons showed changes in activity across the session.

Three distinct activity patterns

A neuron whose firing is related to the variable *fraction of the run* could encode a number of biologically-relevant parameters that themselves vary according to the fraction of the run completed, such as reward proximity and acceleration. It is possible that the *fraction of the run* neurons reach a peak at a specific relative location along the approach trajectory. We

constructed z-normalized heatmaps of each neuron's activity aligned to locomotion onset, peak of acceleration, peak of speed, peak of deceleration and locomotion end (Fig. 3A). Some neurons seemed to be inhibited during the runs, an observation we confirmed by comparing the firing rate during the runs with that during the inter-run intervals. Eleven neurons were significantly inhibited during the locomotion phase (paired t-test, $P < 0.01$) and were named locomotion-off (LOff) cells. An example neuron's histograms are shown in Figure 4A1,2, and heatmaps of all LOff cells are shown in Figure 5A. These heatmaps show that LOff cells tend to be inhibited beginning just prior to locomotion onset, continue to be inhibited throughout the run, and abruptly recover from the inhibition just after locomotion offset (see also the average activity of all LOff cells in Fig. 4A4).

Figure 3A shows that many of the remaining neurons exhibited activity peaks at various times from before locomotion start to after locomotion end. Consequently, the distribution of the heatmap peaks sorted by time from the alignment event formed a diagonal line, particularly when activity was aligned by the peak of speed (roughly the midpoint of the run). To assess whether this diagonal was the result of each neuron's firing consistently reaching a peak at about the same time across runs relative to the peak of speed, we split the data from each neuron into two pools counterbalanced by trial order and target arm. We constructed peak speed-aligned heatmaps of the activity of all neurons calculated with the first data pool, sorted by the time of peak of activity (Fig. 3B1) and heatmaps calculated with the second data pool, sorted in the same order as the first pool (Fig. 3B2). We found that the times of the peak bins determined from the two data pools were correlated ($r = 0.43$, $p < 0.0001$). We also found that for 37 neurons (60%), the firing rates in each time bin within individual runs were also correlated between data pools ($P < 0.01$). These results demonstrate that each individual neuron exhibits peaks at consistent times, and that the times during the run at which these peaks occur vary widely across neurons. Moreover, we sorted the second data pool in the same order but aligned the activity by locomotion start (Fig. 3B3) and locomotion end (Fig. 3B4). Those graphs also show a stable pattern in our data.

Intriguingly, neurons that showed an activity peak in the first part of the approach run (before reaching peak speed; i.e., during acceleration) tended to show a valley in the second part of the run (after peak speed; i.e., during deceleration), and vice-versa (Fig. 3A). We hypothesized that a large subset of neurons exhibited the peak-valley pattern of activity because they reach activity peaks and valleys mostly during acceleration and deceleration, respectively. We named these neurons acceleration-on (AOn) cells. Similarly, we hypothesized that neurons exhibiting the complementary valley-peak pattern reached activity peaks and valleys mostly during deceleration and acceleration, respectively. We named these neurons deceleration-on (DOn) cells. To test these hypotheses, we first had to account for the fact that the durations of the acceleration and deceleration phases were not identical across runs, which means that if firing peaks occurred at a specific fraction of the acceleration or deceleration phase, the peaks would occur at different absolute time points in different runs. Therefore, we time-normalized the firing rate data. In each run, the acceleration period was divided into 10 bins of the same size, and the firing rate in each bin was calculated. The deceleration period was also divided into 10 bins. The approximate average width of the adjusted bins was 150 ms. In addition, 7 bins of 150 ms each were included prior to locomotor start and after locomotor end. Next, the firing rates from all

runs were averaged per bin and z-transformed. Finally, we modeled the peak-valley and valley-peak patterns as the sum of two Gaussian curves (2G model, see Experimental Procedures and Supplemental Fig. S6 for details).

To validate the 2G model, we split the firing rate data from all runs of each neuron into two pools. The first data pool was used to calculate the average activity per bin and the second data pool was used to train the 2G model. Next, we examined whether the activity per bin calculated with the first data pool was significantly correlated with the activity predicted by the 2G model (Pearson correlation, $P < 0.01$). Seventeen AOn cells (27%) and 10 DOn cells (16%) passed this criterion (Fig. 4B,C). The peak firing rate of AOn cells occurred exclusively during the acceleration phase (Fig. 4B4, 5B), whereas the firing rate peak of DOn cells occurred mostly during the deceleration phase, although some neurons peaked after locomotion end (Fig. 4C4, 5C). LOff cells were not modeled with the 2G model, but we plotted the time-normalized firing rates of these neurons in the same way (Fig. 4A4).

These firing modes further refine the GLM results (Fig. 2C,D) showing that *speed* (or *acceleration*) and *fraction of the run* explain a portion of the variance in firing rate. To examine how LOff, AOn and DOn cells encode *speed* and *acceleration*, we plotted the simple correlation coefficients relating firing rate and *speed* against the normalized times at which the peak firing of each neuron occurred (Fig. 6A), and similarly for the firing rate vs *acceleration* correlation coefficients (Fig. 6B). AOn cells tended to have the strongest positive correlation coefficients for both *speed* and *acceleration*, whereas LOff neurons had the strongest negative coefficients for *speed*. DOn cells tended to have the strongest negative correlation coefficients for *acceleration* whereas their coefficients for *speed* were more widely distributed across negative and positive values.

To further confirm these findings based on individual neuronal data, we determined, for each class of neurons (LO, AOn, DOn, and non-categorized), whether the mean GLM β values for *speed*, *acceleration* and *fraction of the run*, as well as the mean r coefficient values for simple correlations between the same variables and firing rate were significantly different from 0 ($P < 0.01$, one-sample t test, Fig. 6C-H). The results showed that AOn cells encoded *speed* with positive coefficients, whereas LOff cells and DOn cells encoded *speed* with negative coefficients (Fig. 6D). The coefficients for *acceleration* were significantly different from zero and positive for the AOn cells and negative for the DOn cells, but not for the LOff cells (Fig. 6F). The coefficients for *fraction of the run* were significantly different from zero and negative for the AOn cells and positive for the DOn cells, but not for the LOff cells (Fig. 6H). These results were recapitulated in the GLM β values for the AOn and LOff cells, but the DOn cells showed β values significantly different from zero only for the *fraction of the run*.

Together, these results indicate that the encoding of *acceleration* and/or *fraction of the run* revealed by the GLM is largely the result of AOn and DOn cells' firing peaks and valleys, whereas encoding of *speed* is largely due to AOn cells' positive correlations of firing with *speed* and LOff cells' negative correlations.

Activity of speed-correlated neurons precedes increases in speed

Our finding that the activity of NAc neurons is correlated with approach speed is in agreement with the hypothesis that NAc neurons promote reward seeking (Nicola, 2007; Salamone and Correa, 2012; Nicola, 2016). If the firing of these neurons is causal to increased speed of reward approach, then increases in speed should reliably follow the activation of these neurons. We tested this prediction with a cross-correlation analysis in which we plotted speed versus time aligned to each spike (Fig. 7A1). On average, the speed peaked 146 ms after the action potential in positively-correlated neurons ($P = 0.0017$, t test for difference from 0, Fig. 7B). In contrast, the peaks of the cross-correlograms of the negatively-correlated neurons were not significantly different from 0 ($P = 0.35$, Fig. 7B). As suggested by Figure 6, AOn cells were the class with the strongest correlation between firing and speed. To verify that the firing of these neurons preceded an increase in speed, we constructed heat maps of LOff, AOn and DOn cells' firing-speed cross-correlations. These plots show that only AOn cells consistently exhibited cross-correlogram speed peaks after the spike (Fig. 7A2). Notably, the cross-correlogram speed minimum tended to follow the spike in DOn cells. These results are consistent with the possibility that the firing of some AOn cells causes an increase in speed during the acceleration phase, whereas the firing of some DOn cells causes a decrease in speed during the deceleration phase.

Place-related activity

To test whether location or reward prediction encoding could account for speed or run fraction encoding, we included variables related to location in the GLM described in Supplemental Table S2. None of these variables were found to contribute significantly to the model's predictive power (Fig. 2C). Moreover, we asked whether any of the recorded neurons could be classified as place cells according to established criteria (Yeshenko et al., 2004). Five AOn and two LOff neurons passed the criteria. However, their tentative firing fields were mainly located on the central platform, the neurons were quite active on other parts of the maze, and their firing fields were quite small compared to those of CA1 place cells recorded on a similar radial eight-arm maze (Xu et al., 2019).

Neuronal classification based on electrophysiological properties

We sorted the recorded neurons into tentative populations of medium spiny neurons (MSNs) and interneurons based on their waveform characteristics and the proportion of the neuron's ISIs > 2 s, similar to previous studies (Berke et al., 2004; Gatica et al., 2022). We identified 17/62 (27%) putative MSNs, 18/62 (29%) putative interneurons, and 27/62 (44%) neurons that were not classified due to their ambiguous properties. The firing rate of putative MSNs was 0.9 ± 0.4 Hz (mean ± SD) and the firing rate of putative interneurons was 16.2 ± 12.6 Hz (mean ± SD). We conclude that 7/11 (64%) LOff cells were putative MSNs, 0/11 (0%) were putative interneurons, and 4/11 (36%) were unclassified; 0/17 (0%) AOn cells were putative MSNs, 9/17 (53%) were putative interneurons, and 8/17 (47%) were unclassified; and that 2/10 (20%) DOn cells were putative MSNs, 3/10 (30%) were putative interneurons, and 5/10 (50%) were unclassified (Supplemental Fig. S7).

Histology

Most of the recorded neurons were in the NAc shell, but a few of them were in the NAc core or in the border between the dorsal and ventral striatum (Supplemental Fig. S8). We found no evidence that the different classes of neurons were anatomically clustered.

Discussion

The present study clarifies how NAc shell neurons represent locomotor parameters when animals approach rewarded locations. Rats had to run long distances (~1.5 m) to approach each reward, which allowed us to determine how firing changes during acceleration and deceleration. Firing primarily reflected the animal's speed as well as its progression towards the movement target.

We included variables related to approach kinematics, timing and movement direction in each neuron's GLM. Only three variables - *speed, acceleration* and *fraction of the run* - were found to contribute significantly to the variance in firing rate of the population of NAc neurons (although because *acceleration* and *fraction of the run* were correlated, *acceleration* was found to contribute to variance only when *fraction of the run* was excluded from the GLMs). The findings that the explanatory variables were related to kinematics, and that the approach speed increased after the firing of AOn cells, suggest that the primary function of NAc neurons in this task is to control the time course of increases and decreases in speed.

Although AOn neurons' activity was strongly related to kinematics, we cannot decipher whether the sequential activity of different AOn cells is triggered by the time elapsed after response initiation, the traveled distance, the distance/time needed to arrive at the reward area, or the fraction of the traveled distance completed, because in our experiment these variables were highly correlated with each other. Future experiments specially designed to disambiguate these factors will be needed to determine whether NAc shell AOn cells' activity is related to timing or to other kinematic parameters. Such disambiguation has been accomplished in other brain regions with varying degrees of success. For example, in explicit timing tasks, neurons in the dorsolateral striatum (DLS) show peak activity at sequential times that varied across neurons (Matell et al., 2003; Gouvea et al., 2015; Mello et al., 2015; Bakhurin et al., 2017; Toso et al., 2021). Similar encoding of the temporal structure of different behavioral behaviors has also been found in other brain structures such as the hippocampus, medial prefrontal cortex, and cerebellum (Lusk et al., 2016), as well as the NAc (Tsutsui et al., 2006; Abela et al., 2015), but see (Liu et al., 1998; Wakabayashi et al., 2004; Acheson et al., 2006; Galtress and Kirkpatrick, 2010).

In the present study, NAc neurons did not encode kinematic parameters in a uniform way, but rather fell into three classes defined by when their firing rates increase or decrease during the run. First, we noted that correlation coefficients relating firing and *speed* were widely distributed across both positive and negative values. Many neurons with negative coefficients were found to be continuously inhibited during locomotion (LOff cells, Figs. 4A, 5A, 6C,D), similar to previously-identified NAc neurons that are inhibited throughout appetitive and consummatory behaviors (Taha and Fields, 2006). However, in LOff cells, firing resumed just after locomotion offset even though animals presumably engaged in

reward consumption at that point. As suggested previously (Taha and Fields, 2006), the inhibitions of LOff cells may gate appetitive behaviors or trigger locomotor approach.

In contrast, many neurons with positive *speed* coefficients were not continuously excited during locomotion, but rather exhibited firing peaks during acceleration and valleys during deceleration (AOn cells, Figs. 4B, 5B, 6A-F). Intriguingly, their firing peaks were distributed throughout the acceleration phase (Figs. 4B4, 6A,B) and did not align precisely to the peak of acceleration (Fig. 5B). These results suggest that each AOn cells are activated when the animal is at a different point along the acceleration trajectory, activation that could control the precise timing of the speed increase during the run. This possibility is supported by our cross-correlation results showing that an increase in *speed* followed a spike in all but one AOn cell (Fig. 7A2).

DOn cells were complementary to AOn cells in that DOn cells exhibited a firing valley during acceleration. However, DOn cells' peaks were not limited to the deceleration phase, but tended to occur just before or sometimes after locomotion offset (Figs. 4C4, 5B, 6A,B). DOn cells did not consistently encode *speed* (Fig. 6A,D), but did tend to show negative correlations with *acceleration* and positive correlations with *fraction of the run* (Fig. 6E-H) - a pattern opposite to that of AOn cells. Thus, AOn and DOn cells together account for much of the *fraction of the run* and *acceleration* encoding identified by the GLM analysis, suggesting that together these neurons report the animal's relative position along the run, or, similarly, the animal's proximity to reward. Alternatively, they may shape the changes in speed at different positions along the run. Finally, the fact that DOn cells tend to fire the most near locomotion offset may mean that these neurons are specialized for some aspect of reaching the end of the run, such as coming to a complete stop or preparing for reward consumption.

Our findings that the firing of many NAc shell neurons was related to both *speed* and *fraction of the run*, and that these neurons exhibited peaks throughout the locomotor trajectory, are remarkably similar to previous observations of DLS and dorsomedial striatal (DMS) neurons in rodents executing spontaneous or task-related locomotion (Rueda-Orozco and Robbe, 2015; Sales-Carbonell et al., 2018; Fobbs et al., 2020). For example, in a study by Sales-Carbonell et al. (2018), head-fixed mice had to run 100 cm in a free-spinning wheel to get drops of sucrose solution. During the runs, most DMS neurons showed peak activity at different times in relation to movement onset, similar to the AOn and DOn cells reported here. Moreover, the activity of these DMS neurons was correlated with running speed on a run-by-run basis. Furthermore, like the LOff cells reported here, another subpopulation of DMS neurons were active just before and just after the locomotion period and were inhibited during the locomotion.

It is possible that during a reward approach run, the AOn- and DOn-like cells recorded in the DMS and NAc act as a locomotion accelerator and brake, respectively. The LOff cells are the more likely candidates to control the onset and termination of the reward approach runs, while the AOn and DOn cells are more likely candidates to control the rat speed during different phases of the run. This hypothesis is in close parallel with the roles proposed for the direct and indirect pathway neurons of the dorsal striatum (Alexander

et al., 1986). In agreement with this hypothesis, previous studies showed that optogenetic activation of the direct pathway neurons in the DMS causes an increase in locomotor activity in mice, whereas the activation of the indirect pathway neurons decreases locomotor activity in freely-moving mice (Kravitz et al., 2010; Freeze et al., 2013). However, calcium imaging and electrophysiological single-unit studies in freely moving mice have shown that both direct and indirect pathway neurons are activated at movement onset, suggesting that their roles are more complex than simply to serve as “go” and “stop” neurons (Barbera et al., 2016; Sales-Carbonell, et al., 2018; Nishimaru et al., 2023). Further studies are needed to pin down the precise behavioral and circuit function of AOn, DOn and LOff cells in both DMS and NAc, as well as to determine their identity (direct vs indirect path).

The observation that NAc and DMS contain neurons that exhibit similar forms of kinematic encoding may mean that joint encoding of speed and locomotor progress is a common theme that spans much of the dorsal and ventral striatum. However, because the afferents to the dorsolateral, ventromedial and ventral striatum are heterogeneous (Haber, 2003) and the NAc shell projects to many non-basal ganglia structures (Zahm and Brog, 1992; Winn et al., 1997; Zahm, 2000), the functional role of this encoding may differ across striatal structures. Moreover, our animals were extremely well trained, and there is some controversy as to the strength of kinematics encoding in the dorsal striatum in less-trained vs well-trained animals, as well as in how kinematics encoding and location of the encoding differs during spontaneous movements vs task-related (e.g., reward-seeking) movements (Rueda-Orozco and Robbe, 2015; Fobbs, et al., 2020; Tunes et al., 2022). Future studies are needed to explore the specific roles of striatal regions in learning and expression of stereotyped locomotor approach behaviors, including determining the extent to which reward prediction influences encoding of kinematics. Such studies should include the NAc core, which has a prominent role in invigorating cued approach (Parkinson et al., 1999; Nicola, 2010; McGinty, et al., 2013; du Hoffmann and Nicola, 2014). One might expect that the core, similar to the shell and DMS, also contains AOn, DOn and LOff cells.

The GLM analysis yielded little evidence that NAc neurons participate in choosing which reward location to approach or determining the route to get there. In particular, the *arm* entered variables reflect the movement target and right turn, left turn, angle-center and head direction reflect movement direction, but the firing of few neurons was influenced by these variables (Fig. 2C,D). Further analysis using LASSO largely confirmed this conclusion although two variables (*trial* and *center distance*) were found to contribute to firing variance in about one third of neurons (Supplemental Fig. S5). Notably, representation of distance from center accords with our observation that AOn and DOn neurons reach firing peaks at specific points in the animal’s speed trajectory, as the animal’s peak speed typically occurs near the center of the maze. Representation of trial may indicate that some NAc neurons are sensitive to variables that may change across the session, such as fatigue, arousal or satiety.

LASSO analysis also showed that many kinematics-encoding neurons may have also represented diverse aspects of movement direction such as arm entered, head direction, and angle of the head with respect to the center of the maze. Importantly, LASSO does not reveal the degree of variance in the firing rate explained by each variable, and the absence of strong effects of removing direction variables from the GLM models suggests that direction

representation may have been weak. Nevertheless, our findings that some NAc shell neurons represent navigation and direction parameters accords with previous studies showing that NAc neurons, particularly in the shell, integrate reward and spatial information in maze tasks (Lavoie and Mizumori, 1994; Floresco et al., 1996; Shibata, et al., 2001; Mulder, et al., 2004; Mulder, et al., 2005; German and Fields, 2007; Ito et al., 2008; Khamassi, et al., 2008; van der Meer and Redish, 2009; van der Meer, et al., 2010; Lansink et al., 2012). Consistent with these observations, hippocampal projections to the NAc shell may be required for spatial navigation towards large rewards (Albertin, et al., 2000). Our rats were overtrained and likely approached reward locations (particularly the second and third run in each trial) in a sequence of habit-like stimulus-action chains (Graybiel, 1995) rather than using a navigational strategy (O'Keefe and Nadel, 1978; Nicola, 2016). Consequently, spatial navigation processing may have been offline or muted.

Our observation of robust anticipatory speed encoding provides a potential mechanism to explain previous observations indicating a role for NAc neurons in promoting reward seeking. Approach speed is an important component of vigor (Floresco, 2015; Salamone et al., 2016; Shadmehr et al., 2016), and increasing dopaminergic (Kalivas and Barnes, 1993; Wu et al., 1993) or glutamatergic activity (Maldonado-Irizarry and Kelley, 1994) in the NAc increases locomotor activity and invigorates reward seeking (Berridge, 2007). Moreover, free-run operant tasks with higher effort requirements are especially susceptible to disruption by interference with NAc dopamine transmission (Salamone, et al., 1999). These effects are due to increased latency to return to the operandum after a pause in which the animal moves away from it (Nicola, 2010). One possibility is that dopamine promotes the firing of NAc AOn cells, which exhibit the most robust positive correlations between firing rate and speed, and whose firing tends to be followed by an increase in speed. The activity of these neurons could then trigger initiation or maintenance of locomotor approach by reaching a threshold. AOn cells could express the D1 receptor as activation of this receptor tends to have excitatory effects (Andre et al., 2010); because DOn cells tend to be inhibited during acceleration, they may express D2 receptors, causing them to be inhibited by dopamine.

One way to test our proposal that kinematic encoding underlies the increased vigor of approach when reward is available would be to systematically vary the reward magnitude and determine how predicted reward magnitude influences kinematics encoding. We were unable to perform such an analysis because we do not have sufficient data from subjects in which different rewards were available in the target arms. We were also unable to compare kinematics encoding on error trials (when an animal enters an unrewarded arm) to rewarded trials because our overtrained animals made so few errors. Thus, although we can confidently conclude that kinematic variables are reflected in the firing of NAc neurons, further studies will be needed to establish whether this encoding is modulated by reward expectation.

Consistent with the idea that AOn cells drive locomotor initiation, previous studies showed that the magnitude of NAc neuronal excitations in response to reward-predictive cues predicts both the latency to initiate approach locomotion and the speed of approach (McGinty, et al., 2013; Morrison, et al., 2017). These cue-evoked excitations are brief

(typically well under 1 s) and precede initiation of movement. Although this time course contrasts with our observation of speed encoding during locomotion, the previous studies used smaller operant chambers in which locomotor events were brief and higher speeds could not be attained. Thus, it is possible that neurons exhibiting cue-evoked excitations are the same as the AOn cells identified here. Conversely, because cue-evoked excitations are greater when the subject is closer to reward (Morrison and Nicola, 2014; Morrison, et al., 2017), it is possible that these neurons are DOn cells because DOn cells tend to exhibit bursts as the animal reaches the rewarded location.

Our results demonstrate that NAc neurons' activity during free-run reward approach is most consistent with control by these neurons over approach kinematics - when to speed up and when to slow down, and by how much.

Supplementary Material

Refer to Web version on PubMed Central for supplementary material.

Acknowledgements

This study was supported by the grants CNPq (432061/2018-5, 306855/2017-8, 465346/2014-60, 314654/2014-3), GACR 20-00939S, and NIH R01DA019473.

Data availability statement

The datasets generated during and/or analysed during the current study are available from the corresponding author on reasonable request.

References

Abela AR, Duan YR, Chudasama Y (2015) Hippocampal interplay with the nucleus accumbens iscritical for decisions about time. European Journal of Neuroscience 42:2224–2233. [PubMed: 26121594]

Acheson A, Farrar AM, Patak M, Hausknecht KA, Kieres AK, Choi S, de Wit H, Richards JB (2006) Nucleus accumbens lesions decrease sensitivity to rapid changes in the delay to reinforcement. Behavioural Brain Research 173:217–228. [PubMed: 16884790]

Albertin SV, Mulder AB, Tabuchi E, Zugaro MB, Wiener SI (2000) Lesions of the medial shell of the nucleus accumbens impair rats in finding larger rewards, but spare reward-seeking behavior. Behav Brain Res 117:173–183. [PubMed: 11099771]

Alexander GE, DeLong MR, Strick PL (1986) Parallel organization of functionally segregated circuits linking basal ganglia and cortex. Annu Rev Neurosci 9:357–381. [PubMed: 3085570]

Ambroggi F, Ghazizadeh A, Nicola SM, Fields HL (2011) Roles of nucleus accumbens core and shell in incentive-cue responding and behavioral inhibition. J Neurosci 31:6820–6830. [PubMed: 21543612]

Andre VM, Cepeda C, Cummings DM, Jocoy EL, Fisher YE, William Yang X, Levine MS (2010) Dopamine modulation of excitatory currents in the striatum is dictated by the expression of D1 or D2 receptors and modified by endocannabinoids. Eur J Neurosci 31:14–28. [PubMed: 20092552]

Atallah HE, McCool AD, Howe MW, Graybiel AM (2014) Neurons in the ventral striatum exhibit cell-type-specific representations of outcome during learning. Neuron 82:1145–1156. [PubMed: 24908491]

Bakhurin KI, Goudar V, Shobe JL, Claar LD, Buonomano DV, Masmanidis SC (2017) Differential Encoding of Time by Prefrontal and Striatal Network Dynamics. J Neurosci 37:854–870. [PubMed: 28123021]

Barbera G, Liang B, Zhang L, Gerfen CR, Culurciello E, Chen R, Li Y, Lin DT (2016) Spatially Compact Neural Clusters in the Dorsal Striatum Encode Locomotion Relevant Information. Neuron 92:202–213. [PubMed: 27667003]

Berke JD, Okatan M, Skurski J, Eichenbaum HB (2004) Oscillatory entrainment of striatal neurons in freely moving rats. Neuron 43:883–896. [PubMed: 15363398]

Berridge KC (2007) The debate over dopamine's role in reward: the case for incentive salience. Psychopharmacology (Berl) 191:391–431. [PubMed: 17072591]

Brog JS, Salyapongse A, Deutch AY, Zahm DS (1993) The patterns of afferent innervation of the core and shell in the "accumbens" part of the rat ventral striatum: immunohistochemical detection of retrogradely transported fluoro-gold. J Comp Neurol 338:255–278. [PubMed: 8308171]

Caref K, Nicola SM (2018) Endogenous opioids in the nucleus accumbens promote approach to high-fat food in the absence of caloric need. Elife 7.

Cousins MS, Atherton A, Turner L, Salamone JD (1996) Nucleus accumbens dopamine depletions alter relative response allocation in a T-maze cost/benefit task. Behav Brain Res 74:189–197. [PubMed: 8851929]

du Hoffmann J, Nicola SM (2014) Dopamine invigorates reward seeking by promoting cue-evoked excitation in the nucleus accumbens. J Neurosci 34:14349–14364. [PubMed: 25339748]

Engelhard B, Finkelstein J, Cox J, Fleming W, Jang HJ, Ornelas S, Koay SA, Thiberge SY, et al. (2019) Specialized coding of sensory, motor and cognitive variables in VTA dopamine neurons. Nature 570:509–513. [PubMed: 31142844]

Floresco SB (2015) The nucleus accumbens: an interface between cognition, emotion, and action. Annu Rev Psychol 66:25–52. [PubMed: 25251489]

Floresco SB, Seamans JK, Phillips AG (1996) Differential effects of lidocaine infusions into the ventral CA1/subiculum or the nucleus accumbens on the acquisition and retention of spatial information. Behav Brain Res 81:163–171. [PubMed: 8950013]

Floresco SB, Todd CL, Grace AA (2001) Glutamatergic afferents from the hippocampus to the nucleus accumbens regulate activity of ventral tegmental area dopamine neurons. J Neurosci 21:4915–4922. [PubMed: 11425919]

Fobbs WC, Bariselli S, Licholai JA, Miyazaki NL, Matikainen-Ankney BA, Creed MC, Kravitz AV (2020) Continuous Representations of Speed by Striatal Medium Spiny Neurons. J Neurosci 40:1679–1688. [PubMed: 31953369]

Freeze BS, Kravitz AV, Hammack N, Berke JD, Kreitzer AC (2013) Control of basal ganglia output by direct and indirect pathway projection neurons. J Neurosci 33:18531–18539. [PubMed: 24259575]

Galtress T, Kirkpatrick K (2010) The Role of the Nucleus Accumbens Core in Impulsive Choice, Timing, and Reward Processing. Behavioral Neuroscience 124:26–43. [PubMed: 20141278]

Gatica RI, Aguilar-Rivera M, Henny P, Fuentealba JA (2022) Susceptibility to express amphetamine locomotor sensitization correlates with dorsolateral striatum bursting activity and GABAergic synapses in the globus pallidus. Brain Res Bull 179:83–96. [PubMed: 34920034]

German PW, Fields HL (2007) Rat nucleus accumbens neurons persistently encode locations associated with morphine reward. J Neurophysiol 97:2094–2106. [PubMed: 17093128]

Gmaz JM, Carmichael JE, van der Meer MA (2018) Persistent coding of outcome-predictive cue features in the rat nucleus accumbens. Elife 7.

Gouvea TS, Monteiro T, Motiwala A, Soares S, Machens C, Paton JJ (2015) Striatal dynamics explain duration judgments. Elife 4.

Graybiel AM (1995) Building action repertoires: memory and learning functions of the basal ganglia. Curr Opin Neurobiol 5:733–741. [PubMed: 8805417]

Groenewegen HJ, Vermeulen-Van der Zee E, te Kortschot A, Witter MP (1987) Organization of the projections from the subiculum to the ventral striatum in the rat. A study using anterograde transport of Phaseolus vulgaris leucoagglutinin. Neuroscience 23:103–120. [PubMed: 3683859]

Haber SN (2003) The primate basal ganglia: parallel and integrative networks. J Chem Neuroanat 26:317–330. [PubMed: 14729134]

Hauber W, Sommer S (2009) Prefrontostriatal circuitry regulates effort-related decision making. Cereb Cortex 19:2240–2247. [PubMed: 19131436]

Ito R, Robbins TW, Pennartz CM, Everitt BJ (2008) Functional interaction between the hippocampus and nucleus accumbens shell is necessary for the acquisition of appetitive spatial context conditioning. J Neurosci 28:6950–6959. [PubMed: 18596169]

Kalivas PW, Barnes CD (1993) Limbic motor circuits and neuropsychiatry. Boca Raton ; London: CRC Press.

Khamassi M, Mulder AB, Tabuchi E, Douchamps V, Wiener SI (2008) Anticipatory reward signals in ventral striatal neurons of behaving rats. Eur J Neurosci 28:1849–1866. [PubMed: 18973599]

Kravitz AV, Freeze BS, Parker PR, Kay K, Thwin MT, Deisseroth K, Kreitzer AC (2010) Regulation of parkinsonian motor behaviours by optogenetic control of basal ganglia circuitry. Nature 466:622–626. [PubMed: 20613723]

Kropff E, Carmichael JE, Moser MB, Moser EI (2015) Speed cells in the medial entorhinal cortex. Nature 523:419–424. [PubMed: 26176924]

Lansink CS, Jackson JC, Lankelma JV, Ito R, Robbins TW, Everitt BJ, Pennartz CM (2012) Reward cues in space: commonalities and differences in neural coding by hippocampal and ventral striatal ensembles. J Neurosci 32:12444–12459. [PubMed: 22956836]

Lavoie AM, Mizumori SJ (1994) Spatial, movement- and reward-sensitive discharge by medial ventral striatum neurons of rats. Brain Res 638:157–168. [PubMed: 8199856]

Liu XQ, Strecker RE, Brener J (1998) Dopamine depletion in nucleus accumbens influences locomotion but not force and timing of operant responding. Pharmacol Biochem Be 59:737–745.

Lusk NA, Petter EA, MacDonald CJ, Meck WH (2016) Cerebellar, hippocampal, and striatal time cells. Curr Opin Behav Sci 8:186–192.

Maldonado-Irizarry CS, Kelley AE (1994) Differential behavioral effects following microinjection of an NMDA antagonist into nucleus accumbens subregions. Psychopharmacology (Berl) 116:65–72. [PubMed: 7862932]

Matell MS, Meck WH, Nicolelis MA (2003) Interval timing and the encoding of signal duration by ensembles of cortical and striatal neurons. Behav Neurosci 117:760–773. [PubMed: 12931961]

McGinty VB, Lardeux S, Taha SA, Kim JJ, Nicola SM (2013) Invigoration of reward seeking by cue and proximity encoding in the nucleus accumbens. Neuron 78:910–922. [PubMed: 23764290]

Mello GB, Soares S, Paton JJ (2015) A scalable population code for time in the striatum. Curr Biol 25:1113–1122. [PubMed: 25913405]

Morrison SE, McGinty VB, du Hoffmann J, Nicola SM (2017) Limbic-motor integration by neural excitations and inhibitions in the nucleus accumbens. J Neurophysiol 118:2549–2567. [PubMed: 28794196]

Morrison SE, Nicola SM (2014) Neurons in the nucleus accumbens promote selection bias for nearer objects. J Neurosci 34:14147–14162. [PubMed: 25319709]

Mulder AB, Shibata R, Trullier O, Wiener SI (2005) Spatially selective reward site responses in tonically active neurons of the nucleus accumbens in behaving rats. Exp Brain Res 163:32–43. [PubMed: 15654593]

Mulder AB, Tabuchi E, Wiener SI (2004) Neurons in hippocampal afferent zones of rat striatum parse routes into multi-pace segments during maze navigation. Eur J Neurosci 19:1923–1932. [PubMed: 15078566]

Nicola SM (2007) The nucleus accumbens as part of a basal ganglia action selection circuit. Psychopharmacology (Berl) 191:521–550. [PubMed: 16983543]

Nicola SM (2010) The flexible approach hypothesis: unification of effort and cue-responding hypotheses for the role of nucleus accumbens dopamine in the activation of reward-seeking behavior. J Neurosci 30:16585–16600. [PubMed: 21147998]

Nicola SM (2016) Reassessing wanting and liking in the study of mesolimbic influence on food intake. Am J Physiol Regul Integr Comp Physiol 311:R811–R840. [PubMed: 27534877]

Nicola SM, Yun IA, Wakabayashi KT, Fields HL (2004) Cue-evoked firing of nucleus accumbens neurons encodes motivational significance during a discriminative stimulus task. J Neurophysiol 91:1840–1865. [PubMed: 14645377]

Nishimaru H, Matsumoto J, Setogawa T, Nishijo H (2023) Neuronal structures controlling locomotor behavior during active and inactive motor states. Neurosci Res 189:83–93. [PubMed: 36549389]

O'Keefe J, Nadel L (1978) The hippocampus as a cognitive map. Oxford: Clarendon Press.

Parkinson JA, Olmstead MC, Burns LH, Robbins TW, Everitt BJ (1999) Dissociation in effects of lesions of the nucleus accumbens core and shell on appetitive pavlovian approach behavior and the potentiation of conditioned reinforcement and locomotor activity by D-amphetamine. J Neurosci 19:2401–2411. [PubMed: 10066290]

Rueda-Orozco PE, Robbe D (2015) The striatum multiplexes contextual and kinematic information to constrain motor habits execution. Nat Neurosci 18:453–460. [PubMed: 25622144]

Salamone JD, Aberman JE, Sokolowski JD, Cousins MS (1999) Nucleus accumbens dopamine and rate of responding: Neurochemical and behavioral studies. Psychobiology 27:236–247.

Salamone JD, Correa M (2012) The mysterious motivational functions of mesolimbic dopamine. Neuron 76:470–485. [PubMed: 23141060]

Salamone JD, Cousins MS, Bucher S (1994) Anhedonia or anergia? Effects of haloperidol and nucleus accumbens dopamine depletion on instrumental response selection in a T-maze cost/benefit procedure. Behav Brain Res 65:221–229. [PubMed: 7718155]

Salamone JD, Yohn SE, Lopez-Cruz L, San Miguel N, Correa M (2016) Activational and effort-related aspects of motivation: neural mechanisms and implications for psychopathology. Brain 139:1325–1347. [PubMed: 27189581]

Sales-Carbonell C, Taouali W, Khalki L, Pasquet MO, Petit LF, Moreau T, Rueda-Orozco PE, Robbe D (2018) No Discrete Start/Stop Signals in the Dorsal Striatum of Mice Performing a Learned Action. Curr Biol 28:3044–3055 e3045. [PubMed: 30270180]

Shadmehr R, Huang HJ, Ahmed AA (2016) A Representation of Effort in Decision-Making and Motor Control. Curr Biol 26:1929–1934. [PubMed: 27374338]

Shibata R, Mulder AB, Trullier O, Wiener SI (2001) Position sensitivity in phasically discharging nucleus accumbens neurons of rats alternating between tasks requiring complementary types of spatial cues. Neuroscience 108:391–411. [PubMed: 11738254]

Sjulson L, Peyrache A, Cumpelik A, Cassataro D, Buzsaki G (2018) Cocaine Place Conditioning Strengthens Location-Specific Hippocampal Coupling to the Nucleus Accumbens. Neuron 98:926–934 e925. [PubMed: 29754750]

Taha SA, Fields HL (2006) Inhibitions of nucleus accumbens neurons encode a gating signal for reward-directed behavior. J Neurosci 26:217–222. [PubMed: 16399690]

Toso A, Reinartz S, Pulecchi F, Diamond ME (2021) Time coding in rat dorsolateral striatum. Neuron 109:3663–3673 e3666. [PubMed: 34508666]

Tsutsui Y, Nishizawa K, Kai N, Kobayashi K (2006) Lesion of the nucleus accumbens dopamine system shortens the lever pressing interresponse time and delays the response initiation in mice. Neurosci Res 55:S195–S195.

Tunes GC, de Oliveira EF, Vieira EUP, Caetano MS, Cravo AM, Reyes MB (2022) Time encoding migrates from prefrontal cortex to dorsal striatum during learning of a self-timed response duration task. Elife 11.

van der Meer MA, Johnson A, Schmitzer-Torbert NC, Redish AD (2010) Triple dissociation of information processing in dorsal striatum, ventral striatum, and hippocampus on a learned spatial decision task. Neuron 67:25–32. [PubMed: 20624589]

van der Meer MA, Redish AD (2009) Covert Expectation-of-Reward in Rat Ventral Striatum at Decision Points. Front Integr Neurosci 3:1. [PubMed: 19225578]

Wakabayashi KT, Fields HL, Nicola SM (2004) Dissociation of the role of nucleus accumbens dopamine in responding to reward-predictive cues and waiting for reward. Behavioural Brain Research 154:19–30. [PubMed: 15302107]

Winn P, Brown VJ, Inglis WL (1997) On the relationships between the striatum and the pedunculopontine tegmental nucleus. Crit Rev Neurobiol 11:241–261. [PubMed: 9336713]

Wu M, Brudzynski SM, Mogenson GJ (1993) Functional interaction of dopamine and glutamate in the nucleus accumbens in the regulation of locomotion. Can J Physiol Pharmacol 71:407–413. [PubMed: 7691389]

Xu H, Baracskay P, O'Neill J, Csicsvari J (2019) Assembly Responses of Hippocampal CA1 Place Cells Predict Learned Behavior in Goal-Directed Spatial Tasks on the Radial Eight-Arm Maze. Neuron 101:119–132 e114. [PubMed: 30503645]

Yeshenko O, Guazzelli A, Mizumori SJ (2004) Context-dependent reorganization of spatial and movement representations by simultaneously recorded hippocampal and striatal neurons during performance of allocentric and egocentric tasks. Behav Neurosci 118:751–769. [PubMed: 15301602]

Zahm DS (2000) An integrative neuroanatomical perspective on some subcortical substrates of adaptive responding with emphasis on the nucleus accumbens. Neurosci Biobehav Rev 24:85–105. [PubMed: 10654664]

Zahm DS, Brog JS (1992) On the significance of subterritories in the "accumbens" part of the rat ventral striatum. Neuroscience 50:751–767. [PubMed: 1448200]

Nucleus accumbens shell neurons reflect kinematics during reward approach

Nucleus accumbens shell neuronal firing correlates with speed

Nucleus accumbens shell neuronal activity predicts changes in speed

Nucleus accumbens shell neuronal firing correlates with path completion

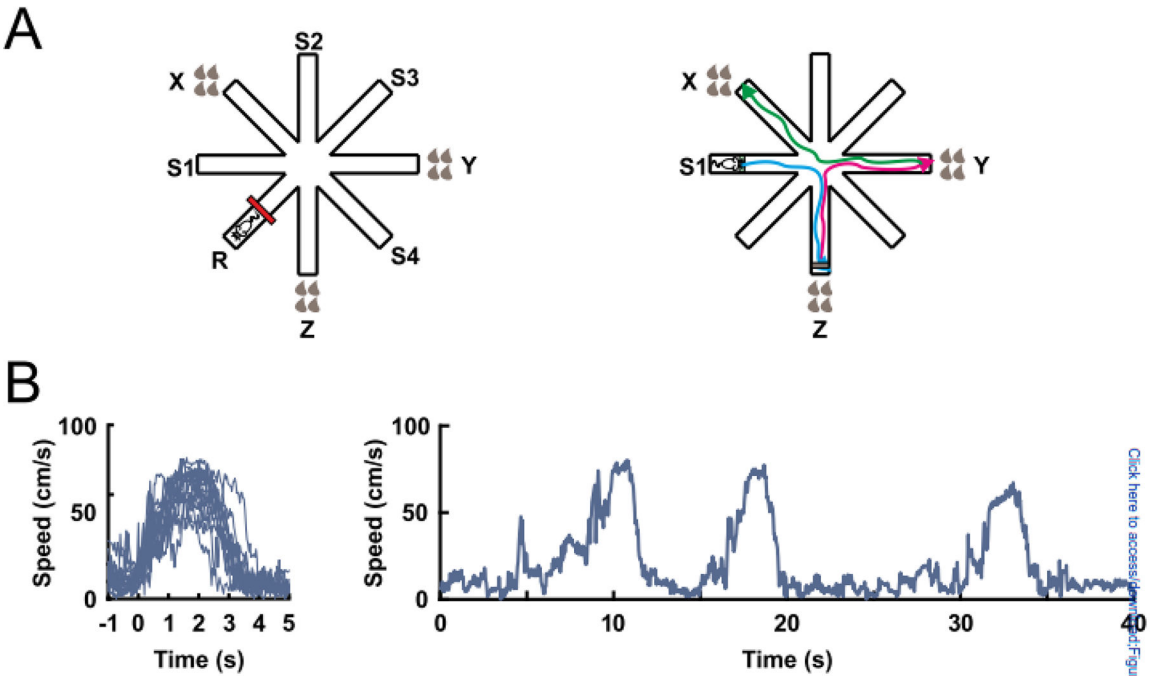

Figure 1:

The eight-arm radial maze task. (A) Rats were trained to find drops of chocolate milk in the ends of the 3 baited arms. Each brown drop represents 25 μl of chocolate milk. The red line represents an obstacle that was placed in the middle of the resting arm between trials to keep the rat restricted in the distal half of the starting arm. S1, S2, S3 and S4 indicate the starting arms (left). A single trial consisted of three subsequent runs (blue, magenta, green) (right). (B) Superimposed changes in *speed* during all runs of an individual session aligned to locomotion start (left). Changes in *speed* during three subsequent runs (right).

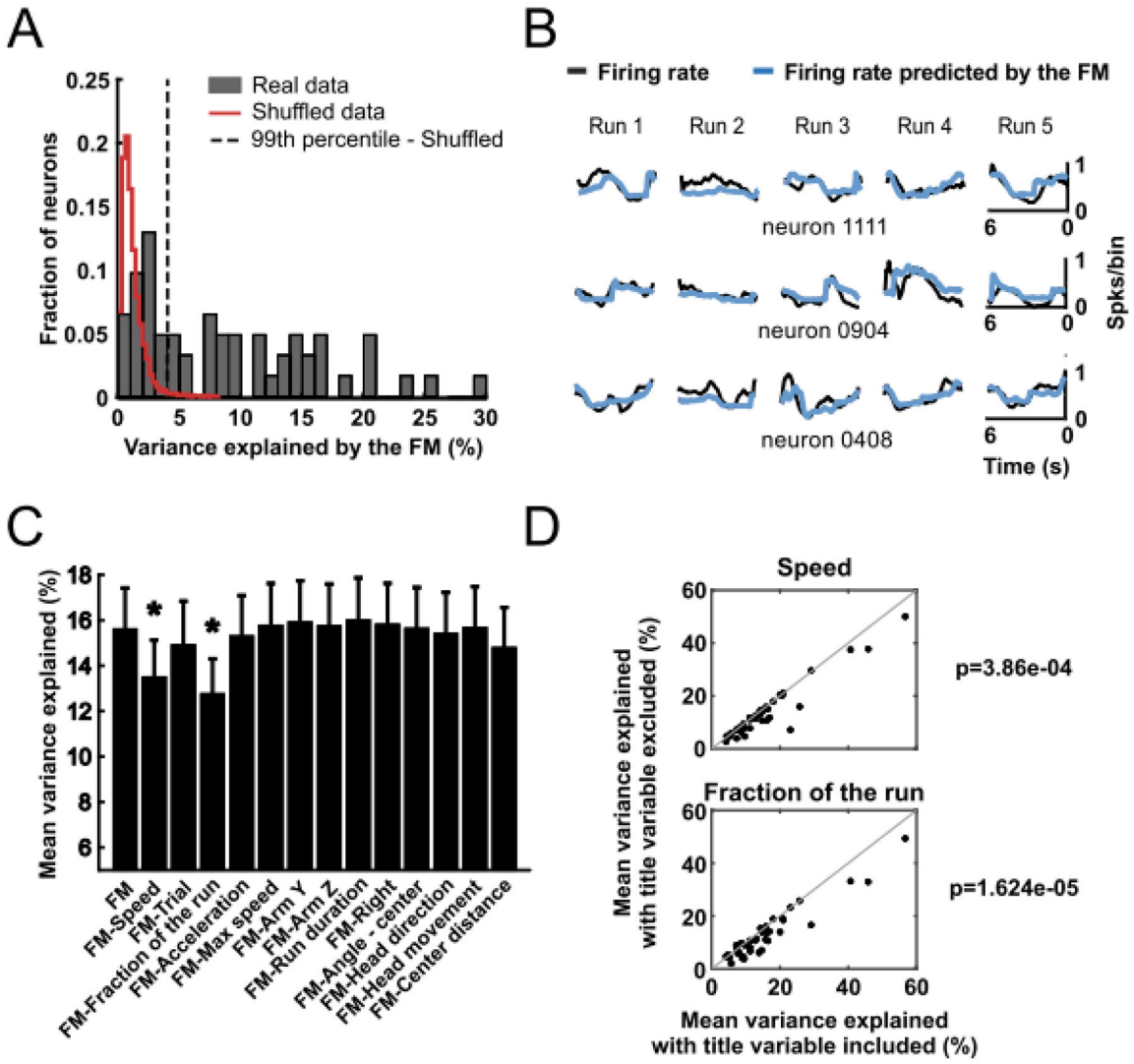

Figure 2:

GLMs were used to predict activity of NAc neurons based on behavioral variables. (A) Distribution of the variance explained by a GLM full model (FM) that used all variables shown in (C) as predictors. Red line delimits the distribution of the variance explained by a GLM calculated with shuffled neuronal data (100 shuffled models per neuron). Neurons to the right of the dashed line (99th percentile of the shuffled models distribution) were classified as significantly explained by the GLM (63% of recorded neurons). In this and subsequent graphs, variance explained is depicted as a percent (100 x r^2_{mean}). (B) Neuronal activity during 5 runs towards the ends of reward arms predicted by the GLM (blue line) compared to the real data (black line) for three individual neurons. (C) Percentage of mean variance explained (mean ± SEM of r^2_{mean} across neurons). Only data from the neurons with activity significantly predicted by the FM (full GLM model) were included. The mean variance explained by the FM is shown in the leftmost column. The other columns show the activity explained by the FM models excluding the indicated variable. * $p < 0.01$, paired t-test (after Bonferroni correction) comparing the indicated model with the FM. (D)

Significant comparisons of mean variance explained by the FM (X-axis) and by the FM after excluding the indicated variable (Y-axis) for all neurons (black dots) explained significantly by the FM. The p-values represent comparison of the mean variance explained by the FM and a model without the particular predictor.

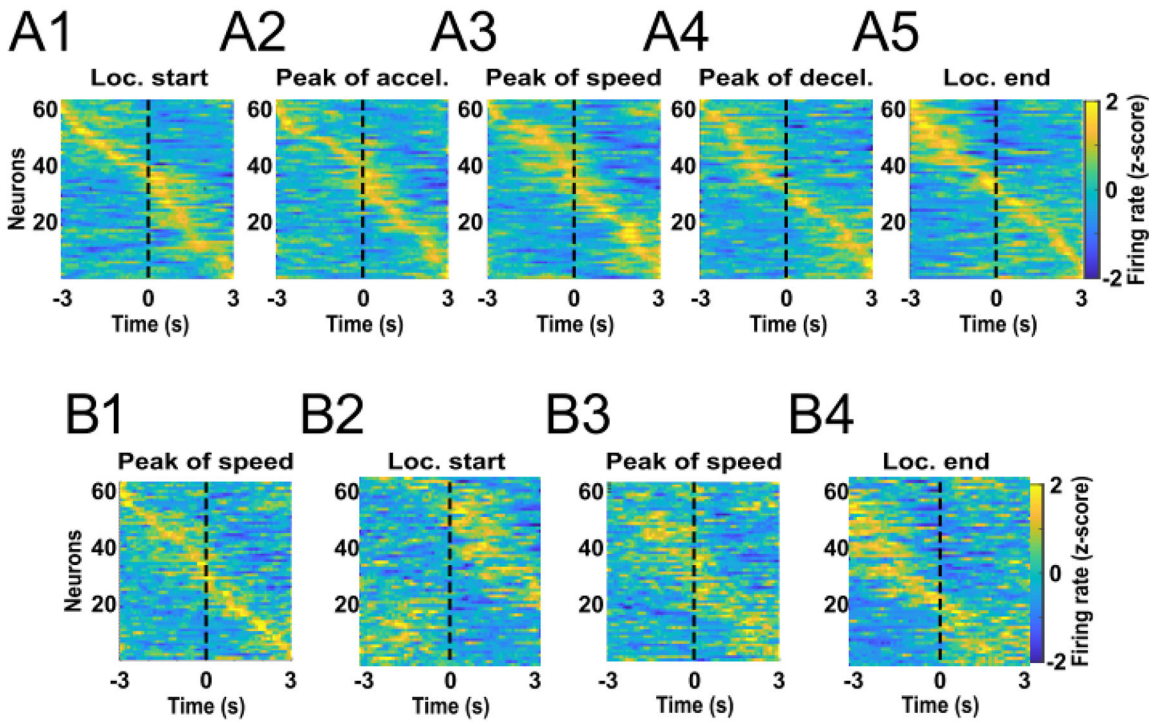

Figure 3:

Different neurons exhibit peak activity at different bins of time. (A) Averaged firing rate z-score heatmaps from all runs of all recorded neurons aligned to locomotion start (A1), peak of acceleration (A2), peak of speed (A3), peak of deceleration (A4), and locomotion end (A5). Neurons were sorted by the time at which the peak activity occurred. (B) Firing rate z-score data from all runs were aligned to the peak of speed and split into two pools counterbalanced for the trial order and visited arm. Neurons were sorted by the peak of activity calculated with the first data pool (B1). The activities of the same neurons calculated with data from the second data pool are shown in the same order as for the first data pool for the locomotion start (B2), peak of speed (B3), and locomotion end (B4) alignments.

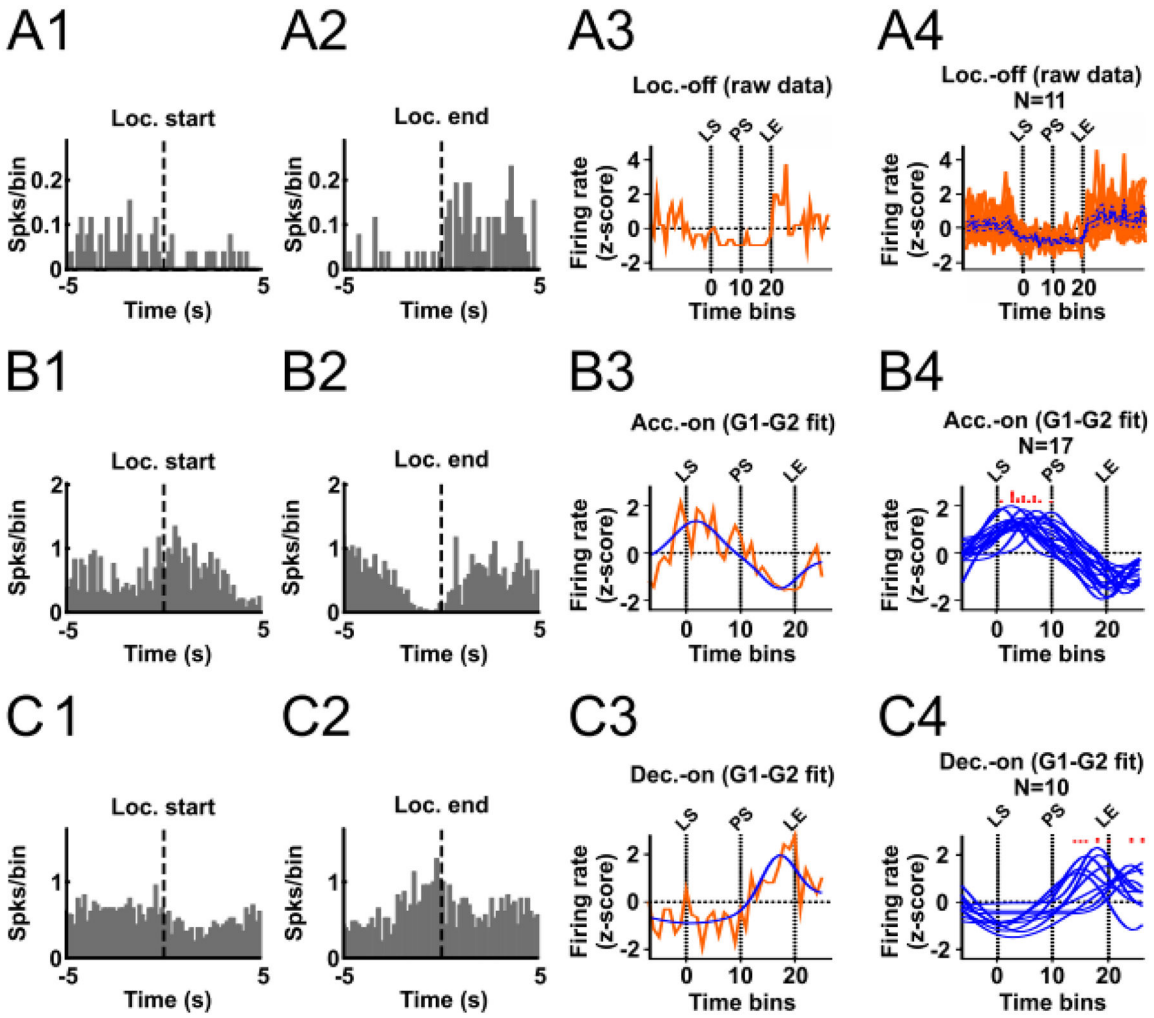

Figure 4:

Classification of LOff, AOn and DOn cells. (A) A1 and A2 show histograms aligned to locomotion start and locomotion end for an example LOff cell. A3 shows the time-normalized histogram for this neuron, and A4 shows time-normalized histograms for all LOff cells superimposed (red traces) and the mean ± SEM (blue trace and blue dashed traces). (B) and (C) show similar plots for AOn (B) and DOn (C) neurons. The blue traces in B3, B4, C3 and C4 show individual neurons' 2G model results. The red histograms superimposed above B4 and C4 indicate the time at which each neuron's peak firing occurs according to its 2G model. LS, PS, and LE correspond to locomotion start, peak of speed, and locomotion end, respectively.

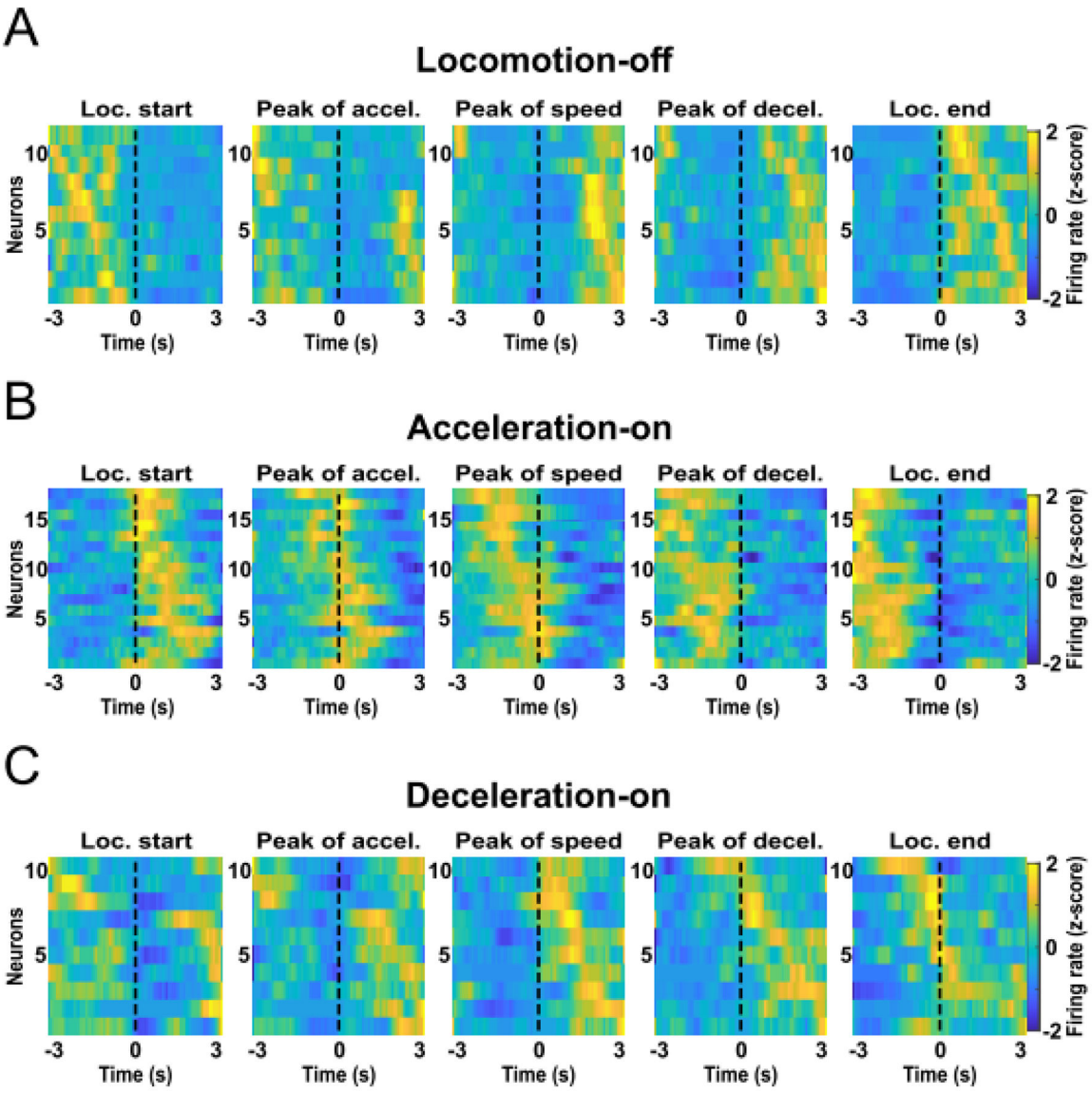

Figure 5:

LOff (A), AOn (B) and DOn (C) cells exhibit peak activity at different kinematic stages of the reward approach run. Heatmaps show firing rates aligned to locomotion start, peak of acceleration, peak of speed, peak of deceleration, and locomotion end. Data were z-scored and the colors in each row show the average across runs for an individual neuron.

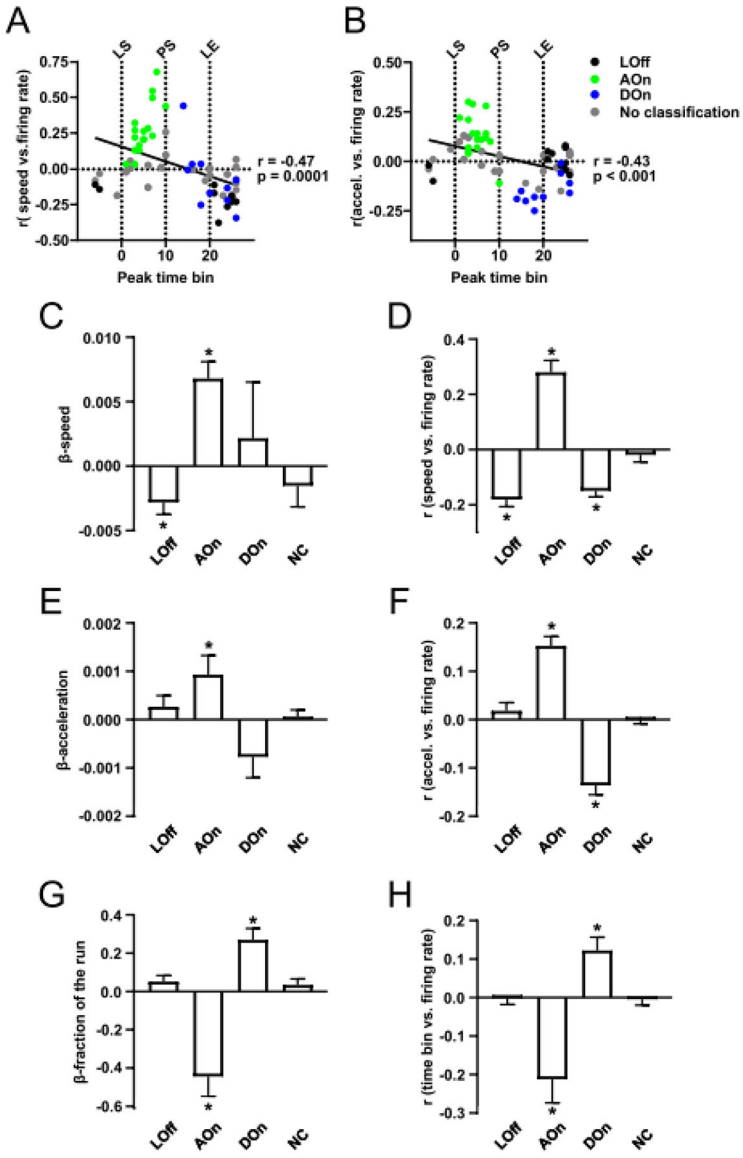

Figure 6:

Neurons in each class defined by the 2G analysis share common correlates to predictors in the GLM analysis. The r values for the correlation between *speed* and firing rate (A) and for *acceleration* and firing rate (B) are plotted against the normalized time at which the neuron exhibits peak firing activity. The time of peak is negatively correlated with both r values; the indicated P values are from Pearson's correlations. Points are color-coded according to classification from the 2G analysis. In (C), (E) and (G), the mean ± SEM weights (β values) from the GLM for the variables *speed* (C), *acceleration* (E), and *fraction of the run* (G) are shown separately for LOff, AOn, DOn and non-categorized neurons. Similarly, in (D), (F) and (H), mean ± SEM r values for simple correlations between these variables and firing rate are shown. * $P < 0.01$, one-sample t-test comparison to 0.

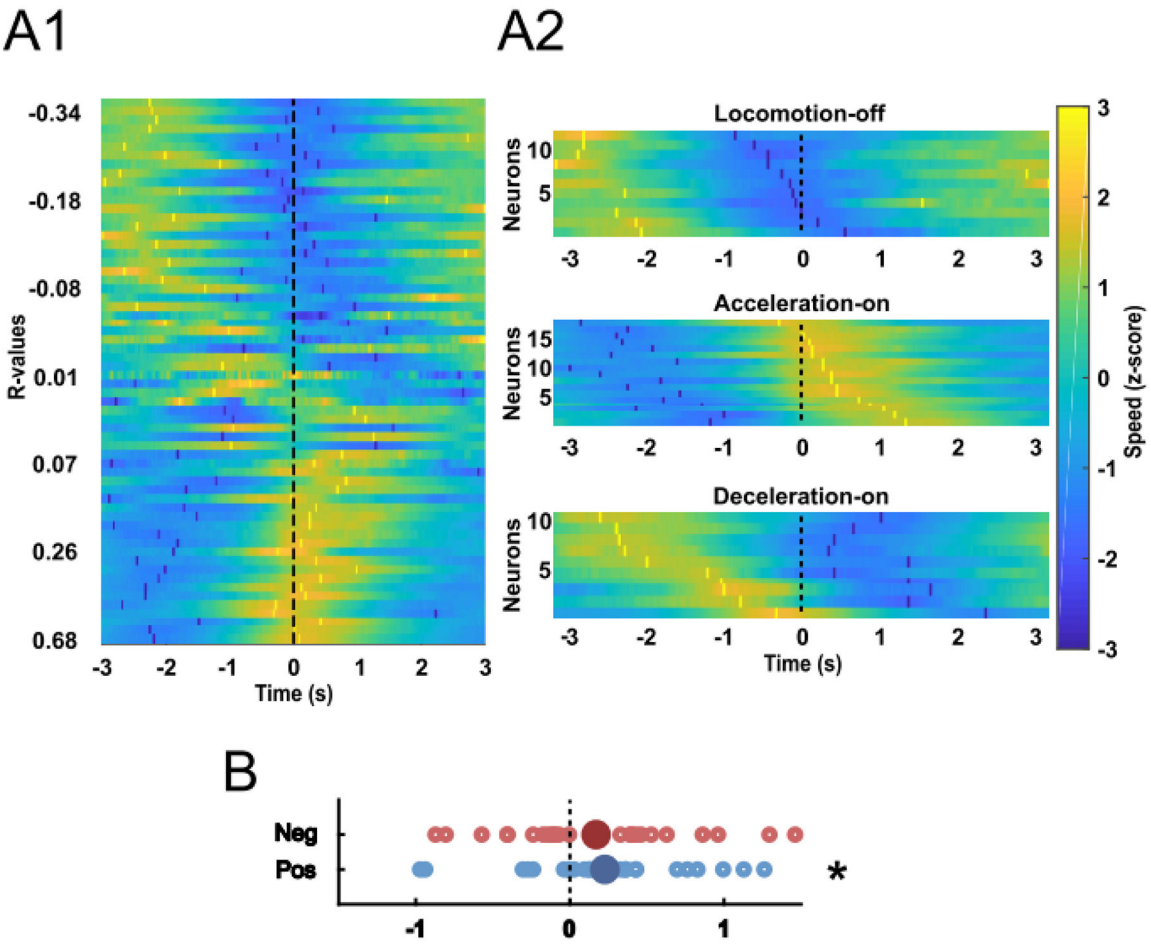

Figure 7:

Spike-speed cross-correlations. (A) Each row in A1 contains a heatmap of the average z-score (colors) of speed aligned to the spikes of an individual neuron. The bright yellow and dark blue markers indicate peaks and valleys of the cross-correlogram, respectively. Neurons in the heat map were sorted according to the Pearson's correlation coefficient (r) for speed vs firing rate. All 62 neurons are shown. In A2, Cross-correlograms are shown separately for LOff, AOn and DOn cells, sorted according to the time at which the cross-correlogram peak speed occurred. (B) The time at which the lowest cross-correlogram speed occurred is shown for neurons that had negative correlations with speed (top, red points), and the time at which the highest cross-correlogram speed occurred is shown for neurons that had positive correlations with speed (bottom, blue points). Only data from the neurons with significant positive (blue) or negative (red) correlations with speed are shown. * P = 0.04, one-sample t test compared to 0.